Electronic structures and transport properties of BN nanodot superlattices of armchair graphene nanoribbons*

An Liping(安丽萍)[1,2] and Liu Nianhua(刘念华)[1,†]

[1]Institute for Advanced Study, Nanchang University, Nanchang 330031, China
[2]Department of Physics, Yanshan University, Qinhuangdao 066004, China

Abstract: The electronic and transport properties of embedded boron nitride (BN) nanodot superlattices of armchair graphene nanoribbons are studied by first-principles calculations. The band structure of the graphene superlattice strongly depends on the geometric shape and size of the BN nanodot, as well as the concentration of nanodots. The conduction bands and valence bands near the Fermi level are nearly symmetric, which is induced by electron–hole symmetry. When B and N atoms in the graphene superlattices with a triangular BN nanodot are exchanged, the valance bands and conduction bands are inverted with respect to the Fermi level due to electron-hole symmetry. In addition, the hybridization of π orbitals from C and redundant B atoms or N atoms leads to a localized band appearing near the Fermi level. Our results also show a series of resonant peaks appearing in the conductance. This strongly depends on the distance of the two BN nanodots and on the shape of the BN nanodot. Controlling these parameters might allow the modulation of the electronic response of the systems.

Key words: graphene nanoribbon; BN nanodot; electronic properties; transport properties
DOI: 10.1088/1674-4926/32/9/092002 **EEACC:** 2520

1. Introduction

Since graphene, a single-atom thick two-dimensional (2D) semimetallic sheet of carbon atoms, was successfully fabricated by mechanical peeling and epitaxial growth[1,2], investigations into the electronic properties of graphene have become a relatively new and thriving area of condensed matter research[3]. Besides understanding the electronic structures of graphene, modifying the electronic structures is another key aspect of interest. One way is to create an antidot superlattice in graphene by means of a regular array of nanoscale perforations[4–9]. Theoretical studies suggest that antidot superlattices can also change the electronic properties of graphene from semimetallic to semiconducting with a significant and controllable band gap. The magnitude of the gap is highly sensitive to the size and separation of the holes. On the other hand, the electronic structures of graphene, as well as nanostructures derived from graphene, can be modified by tuning their chemical components. For instance, hybrid BN and C nanoribbons, which can be viewed as graphene nanoribbons doped with BN nanostructures, exhibit a half-metallic property[10,11].

Recently, graphene doped with BN nanodots has been realized experimentally[12,13]. Despite the experimental progress, few theoretical studies of graphene superlattices doped with periodic BN segments have been reported. The BN-doped graphene superlattice can be regarded as a graphene antidot superlattice but with its antidots filled with BN nanodots, or effectively as a graphene sheet with an external chemical potential. For such a graphene embedded with BN nanodots, how the electronic structures and transport properties of graphene are modified by the BN nanodots remains unclear. It is interesting and important to explore the effect of the BN nanodots on the electronic structure transport properties of graphene superlattices.

In this paper, we consider the BN-doped graphene superlattices, which are essentially the graphene antidots passivated by boron and nitrogen atoms. We present the results of the electronic and transport properties of BN-doped graphene superlattices by using first-principles studies. With the presence of the BN nanodot, the electronic band structures show a wider gap structure that depends on the geometry and size of the BN nanodot, and the new supercell symmetry. In addition, a series of resonant peaks appear in the conductance. This strongly depends on the distance of the two BN nanodots and on the shape of the BN nanodot.

2. Models and computational methods

In our study, the models are embedded boron nitride (BN) nanodot superlattices of armchair graphene nanoribbons (AGNRs) formed by a periodic sequence of BN nanodots modulated by different geometrical shape and size. In Fig. 1, we show the different configurations considered in this study: (a) a hexagon-type BN nanodot with different size, (b) a symmetric rhomboid-type and an asymmetrical rhomboid-type of BN nanodots, and (c) two triangular-type BN nanodots, with B-rich and N-rich, respectively. We designate the superlattice with hexagonal shape as H-B_mN_n, where m and n are the number of B and N atoms, respectively. Similarly, the superlattices with rhomboid and triangular BN nanodots are denoted as R-B_mN_n and T-B_mN_n, respectively. For the cases of H-B_mN_n and R-B_mN_n superlattices, the number of B and N atoms is the same, that is, $m = n$. However, for the case of the T-B_mN_n superlattice, $m > n$ and $m < n$ correspond to B-rich and N-rich edges,

* Project supported by the National Natural Science Foundation of China (No. 10832005).
† Corresponding author. Email: nhliu@ncu.edu.cn
Received 6 April 2011, revised manuscript received 16 May 2011

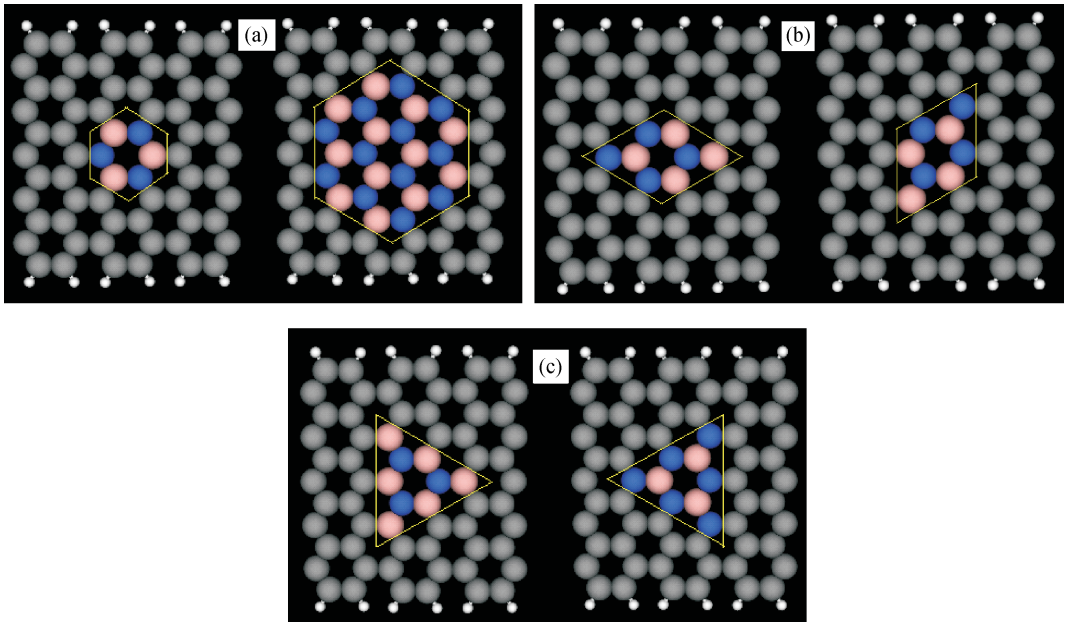

Fig. 1. (Color online) Unit cell of the BN-doped graphene superlattice formed by a N-AGNR including (a) a hexagonal-type BN nanodot (H-B_3N_3 and H-$B_{12}N_{12}$), (b) a symmetric rhomboid-type (R-B_4N_4s) and an asymmetrical rhomboid-type (R-B_4N_4as), (c) triangular-type BN nanodot (T-B_6N_3 and T-B_3N_6). The C, B, N, and H atoms are shown by grey, pink, blue and white balls, respectively.

respectively.

The electronic band structures and transport properties of all nanostructures are calculated by using first principles, based on density-functional theory (DFT) combined with nonequilibruim Green's function (NEGF), as implemented in the ATK package[14, 15]. In our calculations, the exchange correlation potential is described by the Perdew–Zunger local density approximation (LDA-PZ). Single-zata (SZ) basis sets are used. The mesh cutoff is chosen as 100 Ry and a Monkhorst–Pack k-mesh of $1 \times 1 \times 50$ is used. All nanostructures are relaxed using the quasi-Newton method until the absolute value of force acting on each atom is less than 0.05 eV/Å.

The transport properties of the system are calculated using nonequilibrium Green's function formalism. The conductance spectrum is given by the Landauer–Büttiker formalism[16],

$$G = \frac{2e^2}{h}T(E) = \frac{2e^2}{h}\mathrm{Tr}[\Gamma_{\mathrm{L}}G_{\mathrm{C}}^{\mathrm{R}}\Gamma_{\mathrm{R}}G_{\mathrm{C}}^{\mathrm{A}}], \qquad (1)$$

where $T(E)$ is the transmission function of an electron crossing the conductor, $\Gamma_{\mathrm{L/R}}$ is the coupling between the conductor and the respective leads, and $G_{\mathrm{C}}^{\mathrm{R/A}}$ is the retarded (advanced) Green's functions.

3. Results and discussions

3.1. Electronic properties

All structures being studied were relaxed. Figures 2(a)–2(c) show the energy band structures of the three types of BN-doped graphene superlattices, H-B_mN_n, R-B_mN_n and T-B_mN_n, respectively. For an appropriate comparison between these systems, we have considered the same unit cell size for each SL. As a reference, we have included the pristine $N = 11$ AGNR case. All considered H-B_mN_n and R-B_mN_n SLs show a semiconductor electronic behavior with a wider gap structure that depends on the geometry and size of the BN nanodot, and the new supercell symmetry. However, the band gap becomes smaller with increasing lattice constant, which reduces the concentration of BN nanodots in the SL, as shown in Fig. 2(d). In addition, the conduction bands and valence bands near the Fermi level are nearly symmetric, which is induced by electron–hole symmetry. As a result of the additional electronic confining potentials, the band structure of the pristine case is modified. The states at the edge of the Brillouin zone (X point) are changed from the degeneration of pristine to non-degeneration due to the presence of the BN nanodot in each SL. The energy bands for the hexagon-type (H-B_3N_3) and the symmetric rhomboid-type (R-B_4N_4s) BN-doped SL structures show a similar behavior as a function of the longitudinal wave vector k (shown in Figs. 2(a) and 2(b)). This is due to both BN nanodot SLs owning the same specular symmetry with respect to the longitudinal axis of the nanostructure, and the distance from the nanodots to the edges of the AGNR is the same in both cases. On the other hand, the energy dispersions of both considered rhomboid-type BN nanodot SLs are very distinct. Despite the number of BN atoms in both systems being the same, the band structures show great differences, as shown in Fig. 2(b). This is mainly not only due to the lack of specular symmetry with respect to the longitudinal ribbon axis of the asymmetric rhomboid-type SL but also due to the particular geometry of this nanodot, for which the distance of the nanodots with respect to the edges of the ribbon is shorter than that in the symmetric rhomboid-type.

The energy band structures of T-B_mN_n are shown in Fig. 2(c), which illustrates the calculated band structures of the T-B_3N_6 and T-B_6N_3 nanodot SLs. It is interesting to note that the conduction bands and the valence bands near the Fermi levels are inverted for T-B_3N_6 and T-B_6N_3. For instance, the valence bands of T-B_3N_6 are almost identical to the conduction bands of T-B_6N_3, and similarly the conduction bands of

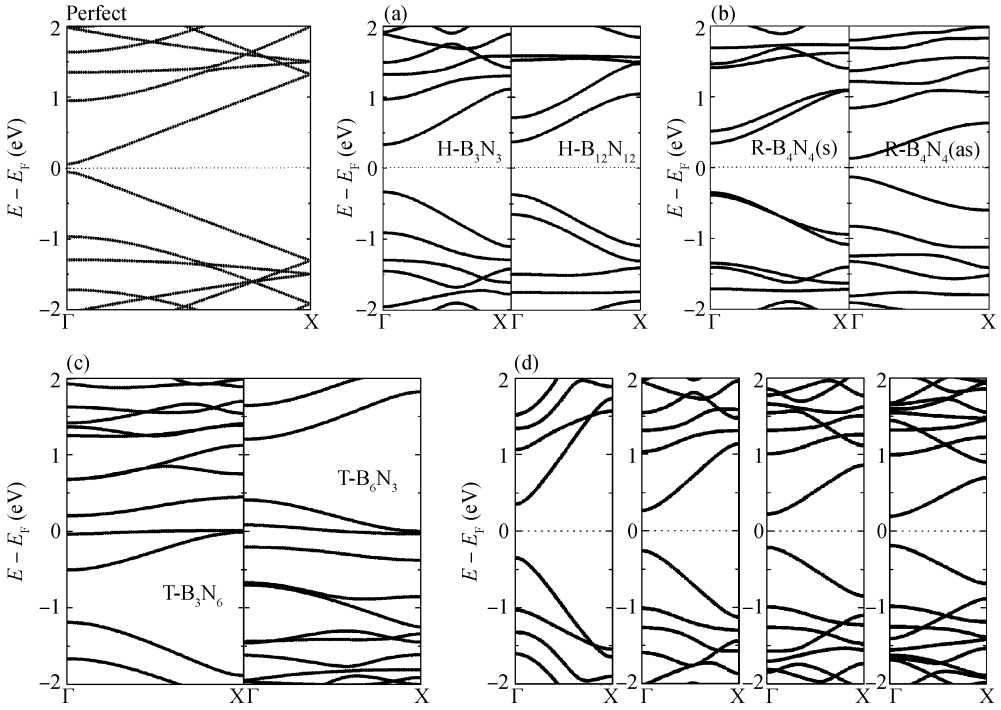

Fig. 2. Electronic band structures of BN-doped graphene superlattices: (a) H-B_mN_n, (b) R-B_mN_n, (c) T-B_mN_n, and (d) for the SLs embedded H-B_3N_3 nanodot with different lattice constants. From left to right, the corresponding constant (energy gap) is two (0.7004 eV), three (0.5268 eV), four (0.4373 eV) and five (0.3861 eV) AGNR primitive-cell lengths, respectively. For comparison, the band structure of pristine $N = 11$ AGNR is given. The Fermi level is set to 0 eV.

T-B_3N_6 are essentially the same as the valence bands of T-B_6N_3. This is easy to understand based on the electron–hole symmetry in graphene systems. For the T-B_mN_n ($m > n$) systems, the electrons are deficient in comparison with the pure graphene, which results in holes in the BN-doped graphene superlattice. In contrast, the T-B_mN_n ($m < n$) structures are rich in electrons. Since the number of redundant electrons in T-B_mN_n ($m < n$) is equal to that of the excess holes in T-B_nN_m, the energy bands of these two complementary structures exhibit the inverted character.

Another interesting observation in Fig. 2(c) is the midgap band. Close to the Fermi level, a very flat band, almost dispersionless in the whole first Brillouin zone, appears in the band structure. The flatness of the band indicates that the corresponding electron state is heavily localized. For the T-B_mN_n, C atoms bond with redundant B atoms or N atoms at the C–B or C–N interface. The mixing of π orbitals of C, B, or N gives rise to bands. The bands near the Fermi level are the bonding C–B (π_B) band and antibonding C–N (π_N^*) band. In addition, the interaction between B–B atoms or N–N atoms is not avoidable. These factors result in the formation of the complicated band structure.

3.2. Conductance properties

Another issue is their transport properties. Therefore we perform transport calculations using the relaxed structures of Fig. 1. In all cases, the graphene nanoribbon structure is divided into three parts: two semi-infinite AGNR leads at the right and left parts, and a central structure, which includes two cases: (1) single or finite periodic arrays of BN nanodots, or (2) two BN nanodots of the same type separated by a variable distance, d. A general scheme of the systems considered is depicted in Fig. 3.

In what follows, the Fermi energy is taken as the zero energy level, and the conductance is written in units of the quantum of conductance $G_0 = 2e^2/h$. Figure 4 shows the behavior of the conductance for the first case, which has a different number of nanodots in the central part. We take an asymmetrical rhomboid-type BN nanodot as an example to calculate the conductance. For reference, the corresponding conductance of the pristine ribbon (dashed line) is included in each one. From Fig. 4(a), we can see that the conductance for the single R-B_4N_4 as nanodot is suppressed, and there is no conductance peak appearing in the first step. However, one remarkable effect that appears for two or more R-B_4N_4 as nanodots is the presence of a series of conductance peaks and gaps at defined energy levels in the conductance, whose number increases with the period number of nanodots, as shown in Figs. 4(b)–4(d). Other types of BN nanodot also have the same results. This is a direct consequence of constructive interference between electron waves scattering the nanodots and propagating back and forth in the conductor region allowing the formation of resonant states. The presence of such resonant states is clearly manifested as peaks in the conductance as a function of the energy. Their properties are related to the shape, size and distance between the nanodots.

In Fig. 5, we present the conductance spectra and the corresponding projected densities of states (PDOSs) for the three types of BN-doped graphene structures considered above for a separation $d = 2$ on a $N = 11$ AGNR. It is clearly seen from Fig. 5 that each conductance spectrum is composed of a series of peaks and also regions where it is completely suppressed in

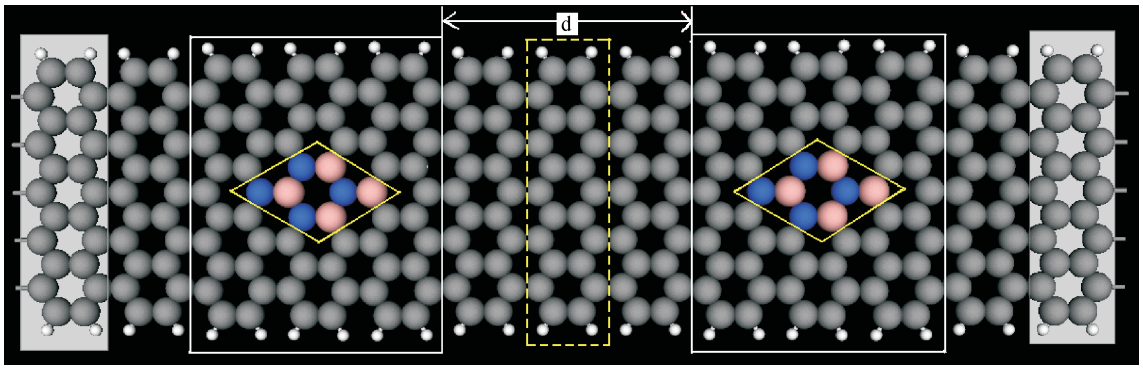

Fig. 3. Schematic view of a two-probe transport system formed by two semi-infinite leads of width $N = 11$ AGNR (shown as white shade regions), and a central conductor including two symmetrical R-B_4N_4 nanodots separated by $d = 3$ measured in units of the AGNR primitive-cell length (2.13 Å) (white dashed rectangle).

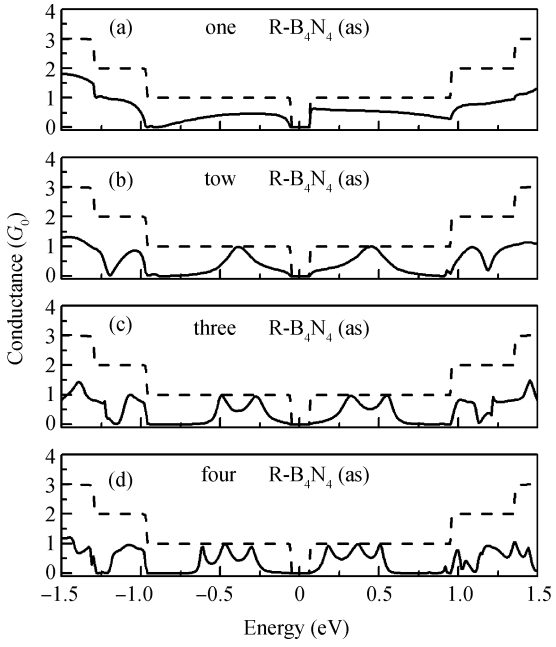

Fig. 4. Conductance as a function of the energy for $N = 11$ AGNR with different numbers of R-B_4N_4 as nanodots: (a) one, (b) two, (c) three and (d) four. The case of a pristine $N = 11$ AGNR is also included (dashed line) for reference.

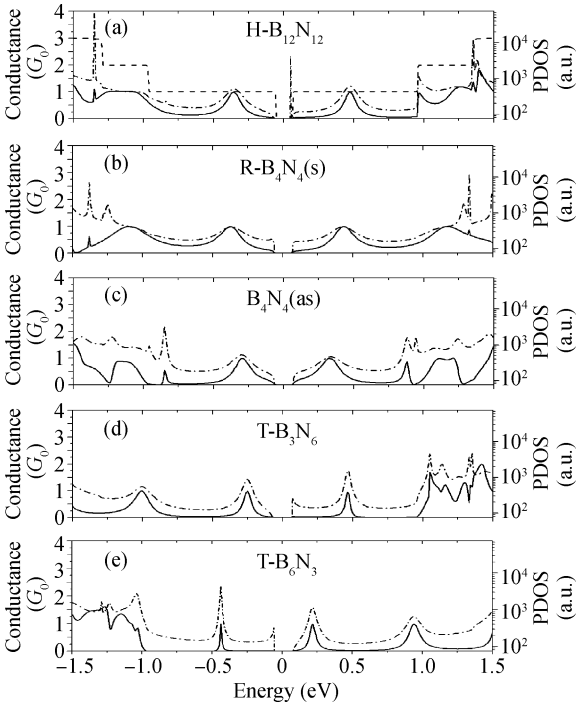

Fig. 5. Conductance (solid lines) and corresponding PDOSs (dash-dot lines) on the electron energy, for two BN nanodots with separation $d = 2$. The conductance of a pristine $N = 11$ AGNR is also included (dash line) in Fig. 5(a) for reference.

the range of low energies, and both the conductance and the PDOS spectra are strongly correlated, especially in the location of their peaks. As discussed before, such a behavior is due to the presence of resonant states in the conductor as a result of the interference among multiple reflections of the electronic wave function between both nanodots. On the other hand, we observe that the position and width of the resonant peak are different for the different BN nanodots. We then conclude that by performing different types of BN nanodot, we can achieve opposite transport effects, which may be of great importance in tuning the electronic response in designed devices.

Results of the conductance as a function of the distance d between two BN nanodots are shown in Fig. 6. This distance is measured in units of the AGNR primitive-cell length. We have considered different values of the distance, e.g. $d = 1, 2, 3, 4,$ and 5. We can observe that for low energies ($|E_F| < 1.0$ eV), the number of peaks increases with the distance between the nanodots. In fact, we also see that these peaks are shifted to lower energies as the distance becomes greater. As the distance increases, more resonant states contribute to the conductance in this energy range. Moreover, when the distance is greater, the resonant peaks are sharper because the electron spends more time inside this region. It is interesting to note that in the high energies ($|E_F| > 1.0$ eV), the conductance shows a strong dependence on the nanodot shape. The effect of the nanodot size can be seen in Fig. 7, which shows the dependence of the conductance on the nanodot size for two H-B_mN_n nanodots. We can see that both structures exhibit resonant peaks, but the width of the peak is different for different sized nanodots. This indicates that the confinement effect is stronger for the larger

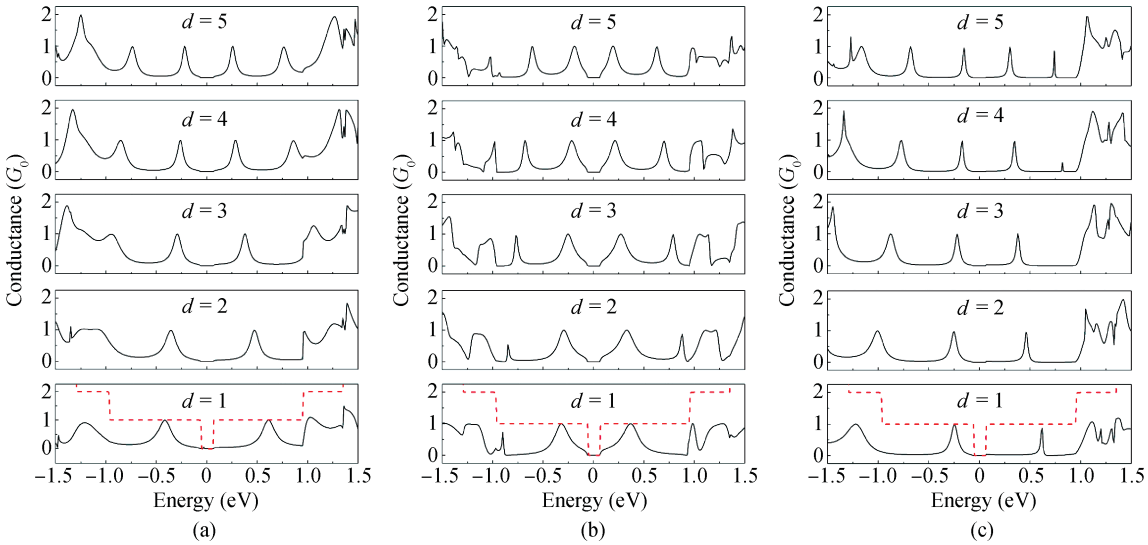

Fig. 6. Conductance dependence on the separation d between two BN nanodots (a) H-$B_{12}N_{12}$, (b) R-B_4N_4as and (c) T-B_3N_6. The case of a pristine $N = 11$ AGNR is also included (dashed line) for reference.

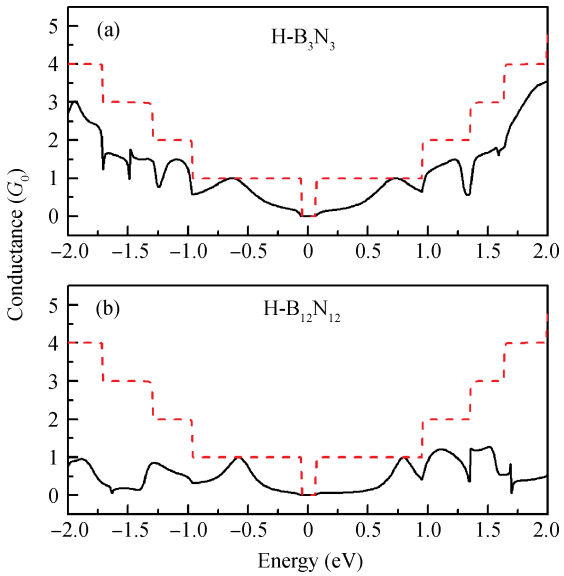

Fig. 7. Conductance dependence on the nanodot size with a fixed distance for (a) H-B_3N_3 and (b) H-$B_{12}N_{12}$. The case of a pristine $N = 11$ AGNR is also included (dashed line) for reference.

nanodot than the smaller one. In particular, for higher energies, the larger nanodot can strongly suppress the conductance, as shown in Fig. 7(b).

The obtained results are similar to the case of transmission through a double (or multiple) quantum barrier(s) system, in which quantum interference phenomena drive the transport, leading to the formation of resonant peaks that are dependent on the barrier geometrical configurations and the distance between them.

Finally, we note that the BN-doped graphene can be produced through a one-step method[12, 13], thus, they are easier to prepare than graphene antidots. In addition, the BN-doped graphene can be more stable than graphene antidots, which are can be easily contaminated by other molecules/atoms.

4. Conclusion

In conclusion, we have performed calculations for the electronic and transport properties of the BN-doped graphene superlattices using first-principles calculations. Our analysis focused on the geometric shape, size and distance of the embedded BN nanodots. The band gap of the graphene superlattice strongly depends on the geometric shape and size of BN nanodots, as well as the concentration of nanodots. An inversion symmetry is observed between the valence bands and the conduction bands with respect to the Fermi level when B and N atoms in the BN nanodot are exchanged. The transport behavior of these systems is defined by the new electronic energy states and forbidden energy regions, which appear due to the extra electronic confinement potential imposed by the embedded BN nanodots in the lattice. A series of resonant peaks are present in the conductance, which depend on the geometrical configurations of BN nanodots and the distance between two nanodots.

Acknowledgments

We wish to thank Atomistix for the use of the trial version of Atomistix ToolKit 2.3 (ATK 2.3).

References

[1] Novoselov K S, Geim A K, Morozov S V, et al. Electric effect in atomically thin carbon films. Science, 2004, 306: 666

[2] Berger C, Song Z M, Li T B. Ultrathin epitaxial graphite: 2D electron gas properties and a route toward graphene-based nanoelectronics. J Phys Chem B, 2004, 108: 19912

[3] Castro Neto A H, Guinea F, Peres N M R, et al. The electronic properties of graphene. Rev Mod Phys, 2009, 81: 109

[4] Pedersen T G, Flindt C, Pedersen J, et al. Graphene antidot lattices: designed defect and spin qubits. Phys Rev Lett, 2008, 100: 136804

[5] Pedersen T G, Flindt C, Pedersen J, et al. Optical properties of graphene antidot lattices. Phys Rev B, 2008, 77: 245431

[6] Fürst J A, Pedersen T G, Brandbyge M, et al. Density functional study of graphene antidot lattices: roles of geometrical relaxation and spin. Phys Rev B, 2009, 80: 115117
[7] Vanevi M, Stojanovi V M, Kindermann M. Character of electronic states in graphene antidote lattices: flat bands and spatial localization. Phys Rev B, 2009, 80: 045410
[8] Liu W, Wang Z F, Shi Q W, et al. Band-gap scaling of graphene nanohole superlattices. Phys Rev B, 2009, 80: 233405
[9] Rosales L, Pacheco M, Barticevic Z, et al. Transport properties of antidot superlattices of graphene nanoribbons. Phys Rev B, 2009, 80: 073402
[10] Dutta S, Manna A K, Pati S K. Intrinsic half-metallicity in modified graphene nanoribbons. Phys Rev Lett, 2009, 102: 096601
[11] Kan E J, Wu X X, Li Z Y, et al. Half-metallicity in hybrid BCN nanoribbons. J Chem Phys, 2008, 129: 084712
[12] Enouz S, Stéphan O, Colliex J L, et al. C-BN patterned single-wall nanotubes synthesized by laser vaporization. Nano Lett, 2007, 7: 1856
[13] Ci L J, Song L, Jin C H, et al. Atomic layers of hybridized boron nitride and graphene domains. Nature Mater, 2010, 9: 430
[14] Brandbyge M, Mozos J L, Ordejon P, et al. Density-functional method for nonequilibrium electron transport. Phys Rev B, 2002, 65: 165401
[15] Taylor J, Guo H, Wang J. *Ab initio* modeling of quantum transport properties of molecular electronic devices. Phys Rev B, 2001, 63: 245407
[16] Datta S. Transport properties of mesoscopic systems. New York: Cambridge University Press, 1995